Positive Position Feedback Control for Large Space Structures

J. L. Fanson*
Jet Propulsion Laboratory, California Institute of Technology, Pasadena, California
and
T. K. Caughey†
California Institute of Technology, Pasadena, California

A new technique for vibration suppression in large space structures is investigated in laboratory experiments on a thin cantilever beam. The technique, called *Positive Position Feedback* (PPF), makes use of generalized displacement measurements to accomplish vibration suppression. Several features of Positive Position Feedback make it attractive for the large space structure control environment. The realization of the controller is simple and straightforward. Global stability conditions can be derived which are independent of the dynamical characteristics of the structure being controlled, i.e., all spillover is stabilizing. Furthermore, the method can be made insensitive to finite actuator dynamics, and is amenable to a strain-based sensing approach. The experiments described here control the first six bending modes of a cantilever beam, and make use of piezoelectric materials for actuators and sensors, simulating a piezoelectric *active-member*. Modal damping ratios as high as 20% of critical are achieved.

Nomenclature

a_1 = $f_a W_a E_a d_{31}(t_a + t_b)$
a_2 = $\frac{1}{2} g_{31} t_s(t_s + t_b)E_b$
B = matrix partition defined in Eq. (A5)
C = matrix of modal coupling coefficients
C_i = curvature coefficient defined in Eq. (15)
D = damping matrix
D_j = $\phi_j'(x_2) - \phi_j'(x_1)$
d_{31} = piezoelectric transverse charge coefficient
E = Young's modulus; matrix defined in Eq. (A4)
E_f = applied electric field
$E^{1/2}$ = $\sqrt{a_1 a_2}\, G^{1/2} C$
G = gain matrix
g = scalar gain
g_{31} = piezoelectric transverse voltage coefficient
I = geometric moment of inertia
j = the imaginary unit (= $\sqrt{-1}$)
M = applied moment
$m(x)$ = mass/unit length of composite beam
N = matrix defined in Eq. (A4)
N_f = number of filters
N_m = number of structural modes
s = Laplace transform variable (= $j\omega$)
t = time coordinate; thickness
x_1 = location of edge of actuator nearest the root
x_2 = location of edge of actuator nearest the free end
y = physical beam deflection
ϵ_E = piezoelectric free strain
ζ = damping ratio (= c/c_{cr})
η = vector of filter coordinates
η = filter coordinate
ξ = vector of modal coordinates
ξ = modal coordinate
σ = uniaxial stress
ϕ = mode shape
ψ = transformed vector of filter coordinates
Ω = modal frequency matrix
ω = modal frequency

Subscripts

i = belonging to the ith mode
f = belonging to filter
a = belonging to actuator
s = belonging to sensor

Introduction

ONE of the predominant difficulties in the theory of large space structure control stems from the fact that large space structures are basically distributed parameter systems. This implies that such structures have a very high number of vibratory modes, often within and beyond the bandwidth of the controller. Usually, there are also modes within the bandwidth that are not targeted for control. The presence of uncontrolled or unmodeled modes within the bandwidth of the closed loop system results in the well-known phenomenon of "spillover."[1] It has long been known that spillover can destabilize residual dynamics, especially at higher frequencies where the dynamics of the structure is least well-modeled.[2] A great amount of research has centered on developing techniques to manage these destabilizing influences.

In the area of structural vibration suppression, the technique with the greatest immunity from the destabilizing effects of spillover is collocated direct velocity feedback, which, in the absence of actuator dynamics, is unconditionally stable.[3,4] In the presence of actuator dynamics, however, instability may result if precaution is not taken. It has been shown that the stability boundary of modes near the natural frequency of the actuator is critically dependent on the inherent natural damping in these modes, a quantity not well-known in most cases.[5]

The technique implemented in this work, *Positive Position Feedback* (PPF), was originally suggested by Caughey and Goh as an alternative to collocated direct velocity feedback.[5] As with velocity feedback, the method is not sensitive to spillover, but, in addition, it is not destabilized by finite actuator dynamics. PPF requires only generalized displacement

Presented as Paper 87-0902 at the AIAA Dynamics Specialist Conference, Monterey, CA, April 9-10, 1987; received April 6, 1988; revision received March 21, 1989.

*Member Technical Staff, Applied Technologies Section. Member AIAA.
†Professor of Applied Mechanics.

measurements that make it amenable to a strain-based sensing approach. Although PPF is not unconditionally stable, as will be seen later, the stability condition is nondynamic. The objective of these experiments is to examine the feasibility of using PPF as a vibration suppression control strategy on a simple beam structure with low inherent bending stiffness, and to investigate the feasibility of using piezoelectric materials as control actuators and strain sensors—simulating a piezoelectric *active-member*.[6]

Positive Position Feedback

The general methodology of PPF is described in Ref. 7. The underlying features can be understood by considering the scalar case. The scalar system consists of two equations, one describing the structure and one describing the compensator:

$$\text{structure:} \quad \ddot{\xi} + 2\zeta\omega\dot{\xi} + \omega^2\xi = g\omega^2\eta \tag{1a}$$

$$\text{compensator:} \quad \ddot{\eta} + 2\zeta_f\omega_f\dot{\eta} + \omega_f^2\eta = \omega_f^2\xi \tag{1b}$$

where g is the scalar gain >0, ξ is the modal coordinate, η is the filter coordinate, ω and ω_f are the structural and filter frequencies, respectively, and ζ and ζ_f are the structural and filter damping ratios, respectively. The compensator is composed of a second-order filter with the same form as the modal Eq. (1a), but with much higher damping ratio. The positive position terminology in the name PPF is derived from the fact that the position coordinate of Eq. (1a) is positively fed to the filter, and the position coordinate of Eq. (1b) is positively fed back to the structure.

A Nyquist stability analysis of this system of equations results in the following necessary and sufficient condition for stability:

$$\text{stability iff:} \quad 0<g<1 \tag{2}$$

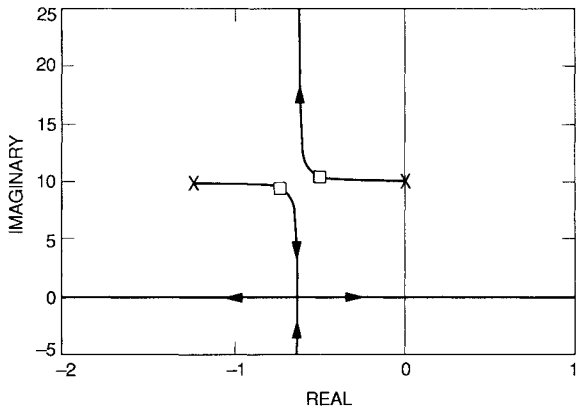

Fig. 1 Root locus of scalar PPF. Boxes indicate design pole locations.

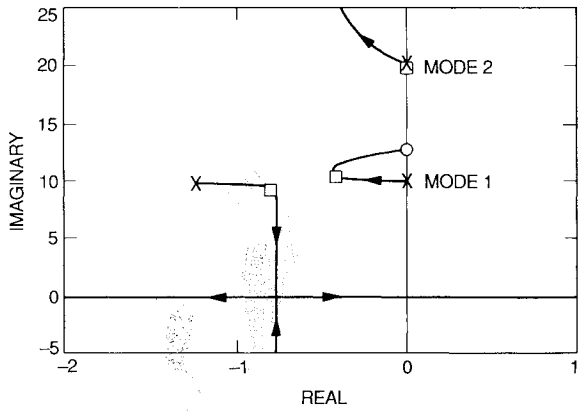

Fig. 2 Uncoupled PPF synthesis with two modes present. Circle indicates transmission zero location.

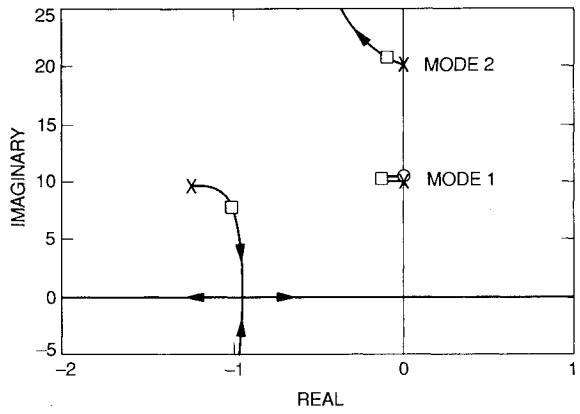

Fig. 3 Uncoupled PPF synthesis with two modes present where the pole and zero nearly cancel.

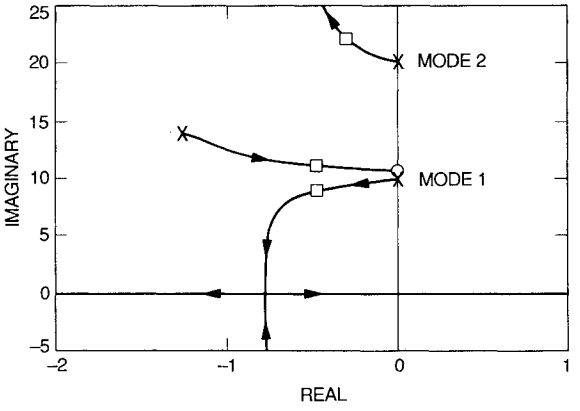

Fig. 4 Example of performance recovery technique where PPF filter frequency is increased.

It is interesting to note that the stability condition does not depend on the damping in the structure. Instability occurs when the stiffness of the structure is made singular by the action of the control. A nondynamic stability criterion is characteristic of PPF. A more complete picture of the behavior of the system in Eqs. (1) can be gained from a root locus plot that traces the movement of the closed-loop eigenvalues (or poles) as a function of gain. Three cases are possible, depending on whether the damped frequency of the filter is greater than, equal to, or less than the damped frequency of the structure. The latter case is shown in Fig. 1.

When more than one mode is present, the root locus for the collocated actuator and sensor resembles Fig. 2, where the circles represent zeros that alternate with the open-loop poles. If the structure is highly flexible, and the sensors and actuators are collocated, residual flexibility may be significant. This residual flexibility results in a strong feedthrough term in the transfer function, which, in turn, can result in very close pole/zero pairs, as shown in Fig. 3. The close pairing alters the character of the root locus, resulting in lower closed loop damping performance. The close pole/zero pairing is exhibited by the test specimen in these experiments, and is to be expected in active-member control of truss type structures. A means of performance recovery in this case is needed.

Rather than resort to techniques that would relocate the zero locations (by altering the sensor placement, for example), we pursued an approach that increases the frequency of the filter pole, again changing the character of the root locus, as shown in Fig. 4. This recovers the closed loop performance. The close proximity of the filter and structural poles tends to make the closed loop pole locations more sensitive to parameter uncertainties, however.

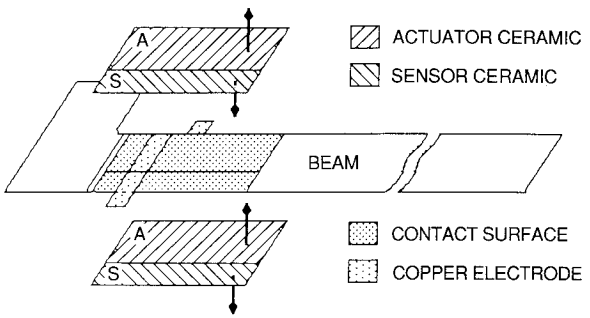

Fig. 5 Layout of piezoelectric ceramics on beam structure.

Design of the Experiment

Uniform Beam Test Structure

For purposes of validating the feasibility of piezoelectric active-member control of a flexible beam,[6] a test structure consisting of a thin aluminum cantilever beam was constructed. Piezoelectric ceramic material was adhered to portions of the beam to simulate the moment-producing effect of active longerons on a space-truss beam. Figure 5 shows the layout of the ceramics on the beam. The ceramic material used was G-1195 PZT, which was adhered to the aluminum beam using cyanoacrylate adhesive.

Two ceramics form the actuator. They are adhered to either side of the beam with their poling geometries arranged such that a common voltage causes one to expand and the other to contract, inducing a bending moment on the composite cross section. Two smaller sensor ceramics are similarly arranged adjacent to the actuator and produce an electric field proportional to the bending strain. Four ceramics form one collocated actuator/sensor pair. Two actuator/sensor pairs were used, as shown in Fig. 6. The actuator/sensor pair located at the root of the beam is labeled Set 1.

The beam was clamped in a support fixture on a small linear bearing table. The table was driven by a 2.5 lb permanent magnet shaker. This enabled various base motion disturbances, such as single frequency sine wave, sine chirp, discrete sine sweep, etc., to study dynamic response and closed loop performance.

Piezoelectric Actuators and Sensors

Piezoelectric material is an inherent electro-mechanical transducer. When an electric field is applied to a piezoelectric, a strain is produced in the material (assuming the boundary conditions are free). Similarly, if the material is stressed mechanically, an electric field is generated.

The material is poled across the thickness, but the induced strain occurs along the length. Ignoring nonideal behavior, the relationship between the applied electric field and the induced free strain for the actuator is given by[8]

$$\epsilon_E = d_{31} E_f \tag{3}$$

where d_{31} is the transverse charge coefficient. The relationship between the applied mechanical stress and the induced electric field is given by[8]

$$E_f = -g_{31}\sigma \tag{4}$$

where g_{31} is the transverse voltage coefficient.

A mechanics analysis results in the following equation for the applied moment from the actuators:[7]

$$M = W_a E_a d_{31}(t_a + t_b) V_a \tag{5}$$

Equation (5) indicates that the applied moment is proportional to the piezoelectric transverse charge coefficient d_{31} and the Young's modulus E_a of the piezoelectric material. Substituting the actual values for the variables gives

$$M = 1.15 \times 10^{-2} V_a \; N \cdot \text{cm/volt} \tag{6}$$

This equation does not account for the compliance of the adhesive used to attach the ceramics, which results in a somewhat lower effective moment due to shear lag.[9] The actuators are assumed to apply a constant magnitude moment across the composite beam cross section everywhere along the length of the actuator.

The sensor ceramics respond to the applied stress, due to bending strain along their length. Assuming small strains, the sensor voltage can be approximated by

$$V_s \propto C\left(\frac{\partial^2 y}{\partial x^2}\right) \tag{7}$$

where $C(\cdot)$ is a functional of distributed curvature along the length of the beam. The simplest assumption is that $C(\cdot)$ is a uniform average of the curvature. This averages the charge density generated pointwise along the ceramic.

Governing Equations

Partial Differential Equation of Motion

The actuator applies a constant moment of magnitude M along its length. Hamilton's Principle is used to derive the governing partial differential equation, using the Bernoulli-Euler beam assumptions on energy. The applied moment $M(x)$ is modeled, using Heaviside step functions as

$$M(x) \propto V_a[h(x - x_1) - h(x - x_2)] \tag{8}$$

The resulting differential equation of motion is

$$m(x)\frac{\partial^2 y}{\partial t^2} + \frac{\partial^2}{\partial x^2}\left(E(x)I(x)\frac{\partial^2 y}{\partial x^2}\right) = \frac{\partial^2 M(x)}{\partial x^2} \tag{9}$$

Substituting Eq. (8) into Eq. (9) and making use of the standard modal expansion

$$y(x,t) = \xi_i(t)\phi_i(x) \qquad \text{(sum on } i\text{)} \tag{10}$$

we obtain

$$m(x)\phi_i\ddot{\xi}_i(t) + \xi_i(t)\frac{\partial^2}{\partial x^2}\left[E(x)I(x)\frac{\partial^2\phi_i(x)}{\partial x^2}\right]$$

$$= a_1 V_a \frac{\partial}{\partial x}[\delta(x - x_1) - \delta(x - x_2)] \tag{11}$$

Multiplying by the mode shape $\phi_j(x)$, integrating over the domain and making use of the fact that the actuators do not span to the ends of the beam, we have

$$\ddot{\xi}_j(t) + \xi_j(t)\omega_j^2 = a_1 V_a[\phi_j'(x_2) - \phi_j'(x_1)] \quad \text{(no sum)} \tag{12}$$

We see that the actuators couple into the modes through the difference in the slopes of the mass-normalized mode shapes at the ends of the actuators. If we define

$$D_j \equiv [\phi_j'(x_2) - \phi_j'(x_1)] \tag{13}$$

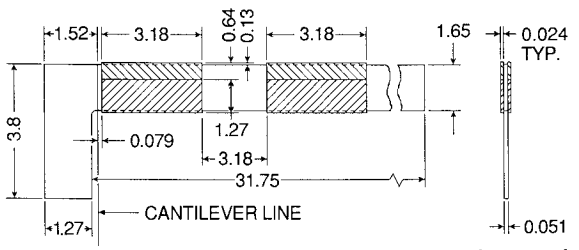

Fig. 6 Actuator/sensor locations on test beam. Dimensions are given in centimeters.

then the modal equations are simply

$$\ddot{\xi}_j(t) + \xi_j(t)\omega_j^2 = a_1 D_j V_a \quad \text{(no sum)} \tag{14}$$

In practice, it was difficult to accurately calculate the D_j, which are slopes of the mode shapes at strong discontinuities in beam section properties.

Substituting Eq. (10) into Eq. (7), we obtain the sensor voltage as a function of modal coordinates and constants C_i.

$$V_s = a_2 \xi_i(t) C \left(\frac{\partial^2 \phi_i(x)}{\partial x^2} \right) = a_2 \xi_i(t) C_i \tag{15}$$

The C_i were also difficult to calculate because the curvature of the mass-normalized mode shapes varied greatly along the length of the sensors, especially near the ends of the ceramics.

Plant Transfer Function

Taking the Laplace Transforms of Eqs. (14) and (15), and assuming zero initial conditions, we obtain the transfer function $P(s)$ between an actuator and a collocated sensor as

$$P(s) = \frac{\hat{V}_s(s)}{\hat{V}_a(s)} = \frac{a_1 a_2 D_1 C_1}{s^2 + 2\zeta_1\omega_1 s + \omega_1^2} + \frac{a_1 a_2 D_2 C_2}{s^2 + 2\zeta_2\omega_2 s + \omega_2^2} + \cdots \tag{16}$$

For the present geometry where there is considerable static flexibility between sensor and actuator, the series in Eq. (16) converges very slowly. This has the effect of making the location of the transmission zeros sensitive to the quasistatic response of all the modes higher in frequency. It also results in the transmission zeros occurring very closely to the lower of the surrounding structural poles. Because of the difficulty in accurately calculating the transmission zero locations, modal models based on measured transfer functions were used in the control synthesis.

Multivariable Stability Criterion for PPF

The general collocated local control implementation of PPF can be written in matrix form as

$$\ddot{\xi} + D\dot{\xi} + \Omega\xi = a_1 C^T G \eta$$

$$\ddot{\eta} + D_f\dot{\eta} + \Omega_f \eta = a_2 \Omega_f C \xi \tag{17}$$

where the vectors and matrices are defined in Appendix A. The stability of the system in Eq. (17) is determined by the following condition, derived in Appendix A:

$$\text{stability iff:} \quad \Omega - a_1 a_2 C^T G C > 0 \tag{18}$$

i.e., positive definite. As in the scalar PPF example of Section II, the stability criterion is nondynamic. It does not depend on the inherent damping in the structure. The gains G must be sufficiently small so as not to cause the stiffness of the structure to become singular.

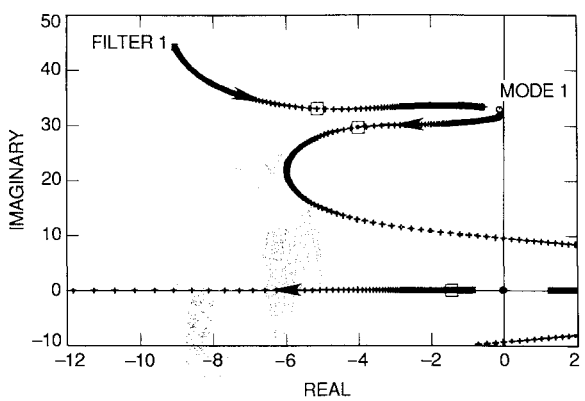

Fig. 7 Root locus for Mode 1 control showing movement of Mode 1 and PPF filter poles.

Table 1 Effect of mode 1 control on modes 1 and 2

	Mode 1			Filter 1		
	ζ_1, %	$\zeta_1\omega_1$	$\zeta_1\omega_1^2$	ζ_{f1}, %	$\zeta_{f1}\omega_{f1}$	$\zeta_{f1}\omega_{f1}^2$
Open loop	0.23	0.0721	2.27	20.00	9.00	405.00
Closed loop	16.30	4.68	135.00	10.40	3.41	112.00
Percent change[a]	7000.00	6400.00	5800.00	—	—	—
Predicted[b]	13.30	3.96	118.00	14.00	4.63	154.00
	Mode 2			Filter 2		
	ζ_2, %	$\zeta_2\omega_2$	$\zeta_2\omega_2^2$	ζ_{f2}, %	$\zeta_{f2}\omega_{f2}$	$\zeta_{f2}\omega_{f2}^2$
Open loop	0.15	0.289	55.50	—	—	—
Closed loop	0.19	0.366	70.30	—	—	—
Percent change[a]	26.70	26.60	26.70	—	—	—
Predicted[b]	0.17	0.320	61.70	—	—	—

[a]Percent change between measured values. [b]Predicted closed-loop values.

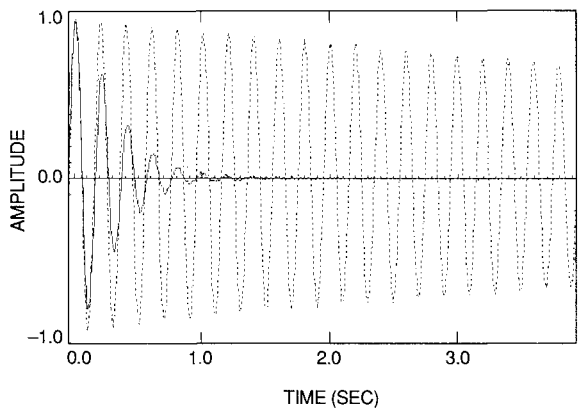

Fig. 8 Open- and closed-loop free decay of Mode 1 under single mode control.

Experiments and Results

Several experiments were performed using one and two sets of actuator/sensor pairs. In the first experiment, one PPF filter was tuned to control the first bending mode at approximately five hertz. Figure 7 shows the root locus for the region near Mode 1. The boxes indicate the design pole locations. The first transmission zero can be seen to occur very close to the Mode 1 pole. The lower manifold of the locus crosses into the right-half plane at a finite frequency, due to nonideal sensor dynamics that were compensated only in the six mode control experiment.[6]

The structure was shaken by step-sine base excitation. The frequency response functions were curve fit to extract the closed loop frequency and damping values. Table 1 summarizes the open-loop and closed-loop damping ratios and damping rates for the structural modes and filter modes. Figure 8 shows the open-loop and closed-loop free decay for Mode 1. The settling time has been reduced from about one minute to about one second.

Three PPF filters were used in a subsequent experiment to control the first three bending modes of the beam. Figures 9 and 10 show the resulting open- and closed-loop frequency response functions for Modes 1-3. The dynamic response is significantly reduced in all the controlled modes. The double-humped shape of the frequency response function near Mode 1 in Figure 9 is due to the pole introduced by the PPF filter.

For the six mode control experiment, the actuator/sensor pair at location 1 (the root of the beam) was used to control Modes 1, 2, and 3; the second pair was used to control Modes 4, 5, and 6. A successive loop closure synthesis approach was

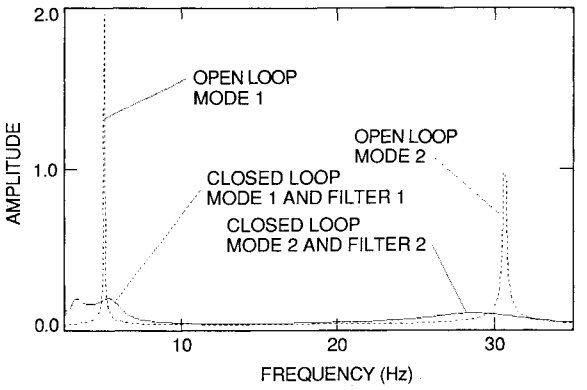

Fig. 9 Open- and closed-loop frequency response functions for Modes 1 and 2. Three mode control case.

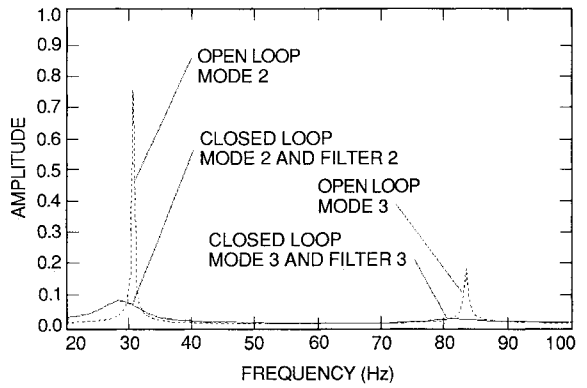

Fig. 10 Open- and closed-loop frequency response functions for Modes 2 and 3. Three mode control case.

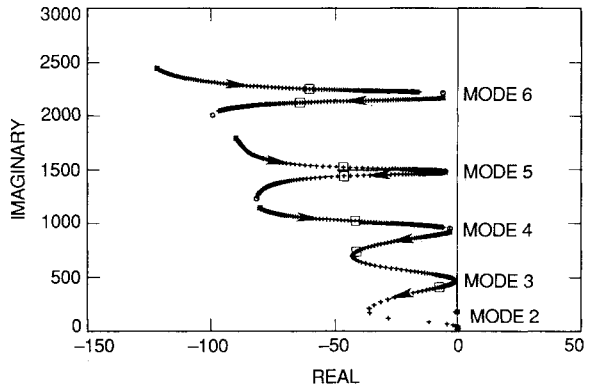

Fig. 11 Root locus for Modes 4, 5, and 6. High-mode control loop at actuator/sensor set 2.

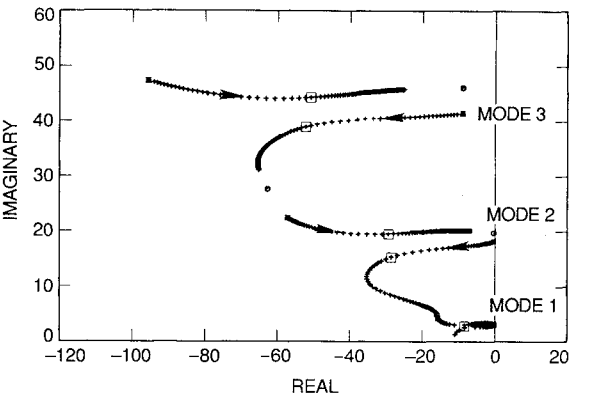

Fig. 12 Root locus for Modes 1, 2, and 3. Low-mode control loop at actuator/sensor set 1.

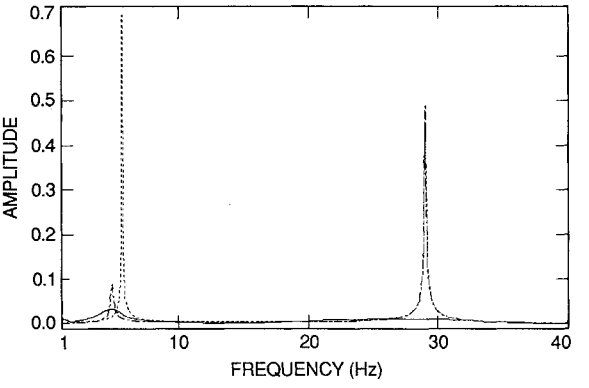

Fig. 13 Frequency response functions for Modes 1 and 2. Six mode control case. Sensor location 1.

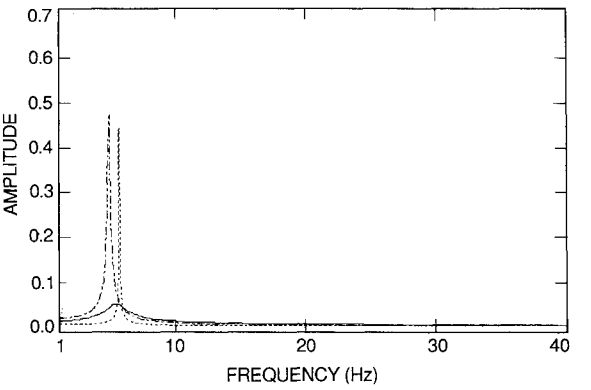

Fig. 14 Frequency response functions for Modes 1 and 2. Six mode control case. Sensor location 2.

followed. The compensator for Modes 4, 5, and 6 was designed first. The closed-loop pole locations for the lower three modes were then used as an initial condition for the design of the compensator for Modes 1, 2, and 3. The sharp rolloff characteristic of the second loop left the higher mode poles unchanged.

The root locus for the Mode 4, 5, and 6 loop is shown in Fig. 11. The Mode 2 pole is unperturbed because the actuator location for the higher mode controller is at a node of Mode 2. Figure 12 shows the root locus for the Mode 1, 2, and 3 loop. The boxes again indicate the design pole locations. The resulting frequency response functions for the region of Modes 1 and 2 are shown in Fig. 13. The dashed line is the open-loop response. The dash-dot-dash line is the response when the higher mode loop is closed. The solid line is the six mode control closed-loop response. Figure 13 shows the response at Sensor 1. It is seen that the downward spillover from the high-mode control is stabilizing to Mode 1. Mode 2 is unperturbed because there is no participation at location 2.

Figure 14 shows the response for the same modes, only this time from Sensor 2 (where the high-mode control is implemented). The dash-dot-dash line indicates that, although the damping of Mode 1 has been increased (a wider half-power bandwidth), the peak amplitude is actually increased slightly over the open-loop peak. This is because the stiffness at this actuator location has been perturbed toward singlularity by the action of the control; the structure has been softened. It is this softening that, if taken beyond the condition expressed in Eq. (18), results in instability. The solid line shows a reduction in response amplitude well below the open-loop peak response as the damping from the Mode 1 PPF pole compensates for the reduction in stiffness.

Table 2 summarizes the six mode control performance. The damping ratios for Modes 5 and 6 fall significantly short of the design values, indicating a performance sensitivity to plant model uncertainties. The Mode 5 and 6 PPF filters are close enough in frequency that they begin to interact with each other, leaving the structural poles near the imaginary axis. It is

Table 2 Six mode control performance

Sensor 1	Mode 1			Filter 1		
	ζ_1, %	$\zeta_1\omega_1$	$\zeta_1\omega_1^2$	ζ_{f1}, %	$\zeta_{f1}\omega_{f1}$	$\zeta_{f1}\omega_{f1}^2$
Open loop	0.33	0.116	4.11	35.00	15.80	709.00
Closed loop	20.00	5.93	176.00	15.00	4.96	164.00
Percent change[a]	6000.00	5000.00	4200.00	—	—	—
Predicted[b]	31.50	8.37	200.00	26.90	8.42	245.00
Sensor 1	Mode 2			Filter 2		
	ζ_2, %	$\zeta_2\omega_2$	$\zeta_2\omega_2^2$	ζ_{f2}, %	$\zeta_{f2}\omega_{f2}$	$\zeta_{f2}\omega_{f2}^2$
Open loop	0.19	0.352	64.10	25.00	57.50	1.32×10^4
Closed loop	24.80	34.00	4.65×10^3	12.00	24.00	4.79×10^3
Percent change[a]	13,000.00	9600.00	7200.00	—	—	—
Predicted[b]	18.60	28.80	4.44×10^3	15.10	29.70	5.84×10^3
Sensor 1	Mode 3			Filter 3		
	ζ_3, %	$\zeta_3\omega_3$	$\zeta_3\omega_3^2$	ζ_{f3}, %	$\zeta_{f3}\omega_{f3}$	$\zeta_{f3}\omega_{f3}^2$
Open loop	0.23	1.05	489.00	20.00	96.00	4.61×10^4
Closed loop	8.00	33.20	1.38×10^4	15.00	68.30	3.11×10^4
Percent change[a]	3400.00	3100.00	2700.00	—	—	—
Predicted[b]	13.40	52.50	2.06×10^4	11.50	51.10	2.27×10^4
Sensor 2	Mode 4			Filter 4		
	ζ_4, %	$\zeta_4\omega_4$	$\zeta_4\omega_4^2$	ζ_{f4}, %	$\zeta_{f4}\omega_{f4}$	$\zeta_{f4}\omega_{f4}^2$
Open loop	0.38	3.54	3.30×10^3	7.00	80.50	9.26×10^4
Closed loop	4.05	29.80	2.19×10^4	2.23	23.40	2.46×10^4
Percent change[a]	970.00	740.00	560.00	—	—	—
Predicted[b]	5.44	41.00	3.08×10^4	4.10	42.10	4.32×10^4
Sensor 2	Mode 5			Filter 5		
	ζ_5, %	$\zeta_5\omega_5$	$\zeta_5\omega_5^2$	ζ_{f5}, %	$\zeta_{f5}\omega_{f5}$	$\zeta_{f5}\omega_{f5}^2$
Open loop	0.39	5.73	8.42×10^3	5.00	90.00	1.62×10^5
Closed loop	0.78	11.40	1.68×10^4	4.97	82.10	1.36×10^5
Percent change[a]	100.00	100.00	100.00	—	—	—
Predicted[b]	3.24	46.90	6.81×10^4	3.04	46.40	7.08×10^4
Sensor 2	Mode 6			Filter 6		
	ζ_6, %	$\zeta_6\omega_6$	$\zeta_6\omega_6^2$	ζ_{f6}, %	$\zeta_{f6}\omega_{f6}$	$\zeta_{f6}\omega_{f6}^2$
Open loop	0.37	7.98	1.73×10^4	5.00	123.00	3.00×10^6
Closed loop	0.62	14.10	3.14×10^4	—	—	—
Percent change[a]	70.00	80.00	80.00	—	—	—
Predicted[b]	3.03	64.70	1.38×10^5	2.67	60.20	1.36×10^5

[a]Percent change between measured values. [b]Predicted closed-loop values.

evident that when the modes become dense it is better to control more than one mode per PPF filter, and it is expected that this will impose limitations on achievable performance, and complications in a coupled synthesis approach.

Conclusions

The laboratory experiments described in this paper have demonstrated the feasibility of using *Positive Position Feedback* (PPF) as a vibration control strategy for flexible structures. Several experiments were performed using one and two sets of piezoelectric actuators and sensors to control up to six structural modes simultaneously. It has been demonstrated that spillover into uncontrolled modes is indeed stabilizing for sufficiently small gain. Modal damping ratios as high as 20% of critical have been achieved on a uniform cantilever beam test structure.

Some observations can be made regarding the implementation of the technique on a very flexible structure. We observed that the residual flexibililty between sensors and actuators due to the low bending stiffness of the beam resulted in close pole/zero pairs. This near cancellation alters the character of the PPF root locus. By increasing the frequency of the PPF filters, closed-loop performance was recovered with the resulting tradeoff that closed-loop pole locations became more sensitive to parameter uncertainties. As the structural modes became densely spaced, it was evident that one PPF filter should be used to control more than one mode.

Appendix A: Positive Position Feedback Stability

Consider the following system of equations that models the general local control case of Positive Position Feedback

$$\ddot{\xi} + D\dot{\xi} + \Omega\xi = a_1 C^T G \eta$$

$$\ddot{\eta} + D_f\dot{\eta} + \Omega_f\eta = a_2\Omega_f C\xi \tag{A1}$$

where the vectors and matrices are defined, as follows:

$\xi \equiv$ modal state vector of length N_m

$\eta \equiv$ filter state vector of length N_f

$G \equiv$ gain matrix—diag. $N_f \times N_f$

$$= \begin{bmatrix} g_1 & & & 0 \\ & g_2 & & \\ & & \ddots & \\ 0 & & & g_{Nf} \end{bmatrix} > 0$$

$C \equiv$ participation matrix—$N_f \times N_m$

$$= \begin{bmatrix} \cdots & \cdots & \cdots \\ \cdots & \text{Full} & \cdots \\ \cdots & \cdots & \cdots \end{bmatrix}$$

$\Omega \equiv$ modal frequency matrix—diag. $N_m \times N_m$

$$= \begin{bmatrix} \omega_1^2 & & & 0 \\ & \omega_2^2 & & \\ & & \ddots & \\ 0 & & & \omega_{Nm}^2 \end{bmatrix} > 0$$

$\Omega_f \equiv$ filter frequency matrix—diag. $N_f \times N_f$

$$= \begin{bmatrix} \omega_{f1}^2 & & & 0 \\ & \omega_{f2}^2 & & \\ & & \ddots & \\ 0 & & & \omega_{fNm}^2 \end{bmatrix} > 0$$

$D \equiv$ modal damping matrix—diag. $N_m \times N_m$

$$= \begin{bmatrix} 2\zeta_1\omega_1 & & & 0 \\ & 2\zeta_2\omega_2 & & \\ & & \ddots & \\ 0 & & & 2\zeta_{N_m}\omega_{N_m} \end{bmatrix} > 0$$

$D_f \equiv$ filter damping matrix—diag. $N_f \times N_f$

$$= \begin{bmatrix} 2\zeta_{f1}\omega_{f1} & & & 0 \\ & 2\zeta_{f2}\omega_{f2} & & \\ & & \ddots & \\ 0 & & & 2\zeta_{fN_f}\omega_{f_{N_f}} \end{bmatrix} > 0$$

The stability criterion for the system in Eq. (A1) is stated in the following theorem.

Theorem A1: *The system in Eq. (A1) is Lyapunov Asymptotically Stable (LAS) iff:* $\Omega - a_1a_2C^TGC > 0$, *i.e., positive definite.*

Proof:

In order that the equations may be symmetrized, it is useful to make the following nonsingular transformation:

$$\eta = \sqrt{\frac{a_2}{a_1}}\, G^{-\frac{1}{2}}\Omega_f^{\frac{1}{2}}\psi \tag{A2}$$

Upon substituting Eq. (A2) into Eq. (A1), and premultiplying the second equation $\sqrt{a_1/a_2}\Omega_f^{-T/2}G^{T/2}$, we have the following pair of equations:

$$\ddot{\xi} + D\dot{\xi} + \Omega\xi = \sqrt{a_1a_2}C^TG^{\frac{1}{2}}\Omega_f^{\frac{1}{2}}\psi$$

$$\ddot{\psi} + D_f\dot{\psi} + \Omega_f\psi = \sqrt{a_1a_2}\Omega_f^{\frac{1}{2}}G^{\frac{1}{2}}C\xi \tag{A3}$$

If we define $E^{\frac{1}{2}} \equiv \sqrt{a_1a_2}G^{\frac{1}{2}}C$, we have the system equation in matrix form as

$$\begin{bmatrix} \ddot{\xi} \\ \ddot{\psi} \end{bmatrix} + \underbrace{\begin{bmatrix} D & 0 \\ 0 & D_f \end{bmatrix}}_{L} \begin{bmatrix} \dot{\xi} \\ \dot{\psi} \end{bmatrix}$$

$$+ \underbrace{\begin{bmatrix} \Omega & -E^{T/2}\Omega_f^{-T/2} \\ -\Omega_f^{\frac{1}{2}}E^{\frac{1}{2}} & \Omega_f \end{bmatrix}}_{N} \begin{bmatrix} \xi \\ \psi \end{bmatrix} = 0 \tag{A4}$$

It is a known result that for $L > 0$, Eq. (A4) is LAS iff $N > 0$.[5] The following establishes that $N > 0$ in Eq. (A4) implies that $\Omega - a_1a_2C^TGC > 0$. (For a proof of sufficiency, see Ref. 7.) For simplicity of notation, we let $B \equiv -E^{T/2}\Omega_f^{T/2}$. If $N > 0$, then

$$[x_1^T\ x_2^T] \begin{bmatrix} \Omega & B \\ B^T & \Omega_f \end{bmatrix} \begin{bmatrix} x_1 \\ x_2 \end{bmatrix} > 0 \tag{A5}$$

for any nonzero x_1 and x_2. Expanding:

$$x_1^T\Omega x_1 + x_2^T\Omega_f x_2 + x_1^TBx_2 + x_2^TB^Tx_1 > 0 \tag{A6}$$

Adding and subtracting $x_1^TB\Omega_f^{-1}B^Tx_1$, we have

$$x_1^T(\Omega - B\Omega_f^{-1}B^T)x_1 + x_1^TB\Omega_f^{-\frac{1}{2}}\Omega_f^{-T/2}B^Tx_1 + x_1^TB\Omega_f^{-T/2}\Omega_f^{\frac{1}{2}}x_2$$

$$+ x_2^T\Omega_f^{\frac{1}{2}}\Omega_f^{-T/2}B^Tx_1 + x_2^T\Omega_f^{T/2}\Omega_f^{\frac{1}{2}}x_2 > 0 \tag{A7}$$

Combining terms

$$x_1^T(\Omega - B\Omega_f^{-1}B^T)x_1 + \underbrace{(\Omega_f^{-T/2}B^Tx_1 + \Omega_f^{\frac{1}{2}}x_2)^T(\Omega_f^{-T/2}B^Tx_1 + \Omega_f^{\frac{1}{2}}x_2)}_{\geq 0} > 0 \tag{A8}$$

Since the second term in Eq. (A8) is only greater than or equal to zero, and the entire expression must be positive, the first term must be positive for any nonzero x_1; therefore,

$$\Omega - B\Omega_f^{-1}B^T > 0 \tag{A9}$$

$$\Omega - a_1a_2C^TGC > 0 \tag{A10}$$

Acknowledgments

The research in this paper was carried out at the Jet Propulsion Laboratory, California Institute of Technology, under a NASA contract.

References

[1]Balas, M. J., "Active Control of Flexible System," *Journal of Optimization Theory and Applications,* Vol. 25, No. 3, 1978, pp. 415-436.

[2]Schaechter, D., "Optimal Local Control of Flexible Structures," *Journal of Guidance and Control,* Vol. 4, No. 1, 1981, pp. 22-26.

[3]Aubrun, J. N., "Theory of the Control of Structures by Low-Authority Controllers," *Journal of Guidance and Control,* Vol. 3, No. 5, 1980, pp. 444-451.

[4]Chen, C. L., "Direct Output Feedback Control of Large Struc-

tures," Dynamics Laboratory Report DYNL-82-1, California Inst. of Technology, Pasadena, CA, 1982.

[5]Goh, C. J. and Caughey, T. K., "On the Stability Problem Caused by Finite Actuator Dynamics in the Control of Large Space Structures," *International Journal of Control,* Vol. 41, No. 3, 1985, pp. 787–802.

[6]Fanson, J. L. and Caughey, T. K., "An Experimental Investigation of Vibration Suppression in Large Space Structures Using Positive Feedback," Dynamics Laboratory Report DYNL-87-1, California Inst. of Technology, Pasadena, CA, 1987.

[7]Caughey, T. K. and Goh, C. J., "Analysis and Control of Quasi-Distributed Parameter Systems," California Inst. of Technology, Pasadena, CA, Dynamics Lab. Rept. DYNL-82-3, 1982.

[8]Jaffe, B., Cook, W., and Jaffe, H., *Piezoelectric Ceramics,* Academic, NY, 1971, pp. 7–10.

[9]Crawley, E. F. and de Luis, J., "Use of Piezo-Ceramics as Distributed Actuators in Large Space Structures," *Proceedings of the 26th AIAA SDM Conference,* 1985.